Journal of CO2 Utilization 96 (2025) 103101

Contents lists available at ScienceDirect

Journal of CO2 Utilization

journal homepage: www.elsevier.com/locate/jcou

Exploitation of seawater brines for the production of Nesquehonite solids and CO_2 utilization

Giuseppe Battaglia, Michela Cardella, Alessandro Tamburini *, Andrea Cipollina, Giorgio Micale

Università degli studi di Palermo, Dipartimento di Ingegneria, Viale delle Scienze, Palermo 90128, Italy

ARTICLE INFO

Keywords:
Magnesium hydroxide
Carbon dioxide
Magnesium carbonate
Bittern
Desalination brine
Carbon utilization

ABSTRACT

The simultaneous utilization of waste CO_2 streams and bivalent rich saline solutions is a crucial opportunity to face climate change challenges. Several authors have investigated desalination seawater brines as promising sources of bivalent solutions for CO_2 utilization technologies. However, the Mg^{2+} and Ca^{2+} content in brines affects the purity of the synthesized compounds. In this context, the present work thoroughly assesses, for the first time, the direct and indirect mineral carbonation processes of real highly concentrated Mg^{2+}-rich saline solutions (bitterns), the latter being the by-products of the evaporation process of seawater or desalination brines in saltworks or evaporative ponds. For comparison, the indirect carbonation process of real desalination brines was also explored. The bittern had Mg^{2+} and Ca^{2+} concentrations of ~2.00 mol/L and ~0.004 mol/L, while ~0.13 mol/L and ~0.025 mol/L were those in the desalination brine, respectively. Carbonation tests were conducted at room temperature and atmospheric pressure in a (semi-)batch reactor. The high concentration of Mg^{2+} and the almost absence of Ca^{2+} in the bittern allowed (i) the production of highly pure Nesquehonite solids (purity ~99 %) and (ii) almost doubling the CO_2 yield (from 23 % to 37 %) through the direct carbonation approach against the indirect one.

1. Introduction

The massive emission of Greenhouse gases (GHGs) has been causing an increase in the global temperature of our planet. Since 1850–2020, global surface temperature has risen by ~1.1°C [1]. Carbon dioxide (CO_2) and methane (CH_4) are the two main GHGs affecting Earth's environment. On the one hand, CH_4 molecules absorb more radiation than CO_2, on the other hand, CO_2 emissions are much higher than methane ones [2]. In 2020, the European Union approved the European Green Deal program with the aim of making European Union (EU) climate-neutral in 2050 [3]. This has pushed research toward innovative, circular and green technologies to satisfy the increasing energy, water and material demand. Desalination and carbon capture storage/utilization (CCS/U) technologies are two promising opportunities to achieve the European Green Deal. Desalination is the leading process in providing fresh water to countries suffering water scarcity. However, desalination produces large amounts of concentrated waste saline solutions, rich in bivalent metallic cations, such as magnesium (Mg^{2+}) and calcium (Ca^{2+}), whose disposal has posed environmental concerns [4]. Carbon capture storage and utilization (CCS and CCU) technologies aim to either store CO_2 or convert it into chemicals or valuable compounds. CCU processes involve the conversion of CO_2 into thermodynamically stable alkaline-earth carbonates by using solutions with a high content of metallic cations [5,6]. With this respect, waste saline solutions produced by industrial desalination activities are the perfect sources to produce high added-value compounds through CCU technologies [7,8]. Among CCU processes, mineral carbonation can be divided into direct and indirect approaches [9,10]. In direct carbonation, CO_2 is injected into a concentrated metallic cations-rich solution along with an alkaline reactant. Indirect carbonation comprises (i) the precipitation of free metallic cations mainly in hydroxide compounds and then (ii) the conversion of hydroxides into carbonate solids through CO_2 injection [7]. Several authors have investigated the possible use of seawater brines for the synthesis of Mg-based compounds via CO_2 utilization. It is worth noting that, Mg-based compounds, such as magnesium hydroxide, $Mg(OH)_2$, nesquehonite, $MgCO_3 \bullet 3H_2O$, or hydromagnesite, $Mg_5(CO_3)_4(OH)_2 \cdot 4(H_2O)$, are currently produced from Mg-bearing minerals. Nesquehonite is adopted as a green building material,

* Corresponding author.
E-mail address: alessandro.tamburini@unipa.it (A. Tamburini).

https://doi.org/10.1016/j.jcou.2025.103101
Received 11 January 2025; Received in revised form 1 March 2025; Accepted 27 April 2025
Available online 5 May 2025

among other applications [11–13], while hydromagnesite is mainly employed as a flame retardant filler in polymeric materials [14]. At atmospheric pressure, nesquehonite crystallization occurs at relatively low temperatures (up to 60 °C), while hydromagnesite is favoured above 60°C [12,15]. Cheng et al. [16] studied the influence of the temperature on the crystallization process of magnesium carbonate hydrates from magnesium chloride ($MgCl_2$) solutions (0.5 mol/L) mimicking the Mg concentration of Qinghai salt lakes (China). Sodium carbonate was used as alkaline reactant. Nesquehonite crystals with a needle-like morphology were obtained in the temperature range 0° and 40°C, while hydromagnesite crystals were formed over temperatures ranging of 60°-90°C. Wang et al. [17] investigated the possible application of several aqueous sources, such as concentrated seawater brines, for CO_2 utilization through the reaction with Ca^{2+} and Mg^{2+} ions. Theoretical analyses indicated that the carbonation reaction could be favoured by increasing the reaction pH and/or the CO_2 partial pressure. Experiments conducted by using synthesized seawater brines confirmed this possibility. Singh et al. [18] investigated the indirect carbonation process of seawater desalination brines through the precipitation of $Mg(OH)_2$ solids via the addition of calcium oxide and the further injection of a CO_2 stream. The mechanical properties of synthesized partially carbonated $Mg(OH)_2$ solids were analysed for their potential use as a construction material. Singh and Celik [19] also explored the carbonation and strength development of brucite recovered from desalination reject brine by supercritical carbon dioxide curing process. Bang et al. [20] proposed a two-stage CO_2 mineralization process of desalination brines in order to produce high purity solids avoiding the simultaneous co-precipitation of Ca- and Mg-compounds. More precisely, sodium hydroxide (NaOH) solutions were firstly employed to precipitate Mg^{2+} in the form of $Mg(OH)_2$ solids. Then, $Mg(OH)_2$ solids were carbonated as hydromagnesite, while the remaining liquid phase was treated with CO_2 and NaOH solutions to precipitate $CaCO_3$ solids.

Apart from seawater brines, bitterns are attractive Mg^{2+} rich sources. Bitterns are highly-concentrated saline solutions generated in ponds or saltworks after the evaporation of seawater or seawater brines. The Mg^{2+} concentration in bitterns can be up to 50 times that in seawater, while the concentration of Ca^{2+} is almost negligible thanks to the selective evaporation process occurring in the evaporative ponds that leads to the preliminary precipitation of Ca-based compounds. The high concentration of Mg^{2+} in the bitterns allows the use of these solutions also for direct carbonation processes. Pan et al. [21] explored a novel environmentally friendly process for the utilization of oyster shells and waste bittern, by product of salt production, to produce nesquehonite and calcium chloride. An organic extraction phase comprising Tri (octyl-decyl)amine (R3N), isoamyl alcohol and CO_2 was employed. Zhang et al. [22] proposed a facile and cost-effective method to completely transform Mg^{2+} to hydromagnesite via carbon dioxide (CO_2) mineralization from synthetic bitterns. Synthetic bittern solutions with Mg^{2+} concentration of 2.2 mol/L were let to react with NaOH and CO_2 stream via direct carbonation at 70°C. The synthesized hydromagnesite solids were tested for uranium extraction applications. Lu et al. [23] studied the indirect CO_2 mineralization process of concentrated synthetic Mg^{2+}-rich solutions using ammonium bicarbonate, NH_4HCO_3, in the presence of sodium alginate. The authors aimed at providing insights into the preparation of hierarchically structured hydrated magnesium carbonate compounds in order to reduce the cost of the entire CO_2 capture process.

The present work, for the first time, systematically examines the possible exploitation of real bittern solutions and their direct and indirect carbonation process, aiming at producing highly pure nesquehonite solids through the utilization of CO_2 sources. For the sake of comparison, the indirect carbonation process of seawater desalination brines was also investigated. The research has been developed in the framework of the activities of the Horizon 2020 European projects REWAISE and SEArcularMINE [24,25]. In the REWAISE project, the use of evaporation ponds is proposed as an effective step to valorise desalination brines by producing chemicals, such as NaCl or calcium-based compounds, and Ca^{2+}-free bitterns, suitable for the production of highly pure magnesium compounds [26,27]. The SEArcularMINE project aimed at developing a novel innovative integrated process for the recovery of critical raw materials through the valorisation of saltworks bitterns. In the present work, two different Mg-rich aqueous solutions were adopted: (i) a seawater desalination brine produced by the desalination plant in Tenerife Island (Spain) that was enriched in bivalent ions after a nanofiltration (NF) step, and (ii) a real bittern solution collected from the Margi saltworks located in the Trapani district (Sicily, Italy).

2. Materials and methods

2.1. Saline solutions and reagents

In the experimental campaign two saline solutions were employed: (i) a reverse osmosis (RO) brine enriched in bivalent ions after a NF stage and (ii) a saltworks bittern. The brine was collected from the RO desalination plant located in Tenerife island (Canary islands, Spain) and further concentrated in bivalent ions through a NF step (i.e. the NF retentate was employed), while the bittern came from the Margi saltworks located in Trapani district (Italy). Table 1 reports the concentration of the main cations dissolved in the saline solutions measured by Ion chromatography (IC, Metrohm model 882 compact IC plus), and the concentration of bicarbonate species measured by titration following the APAT 2010 B method (1/50 N sulfuric acid was used as the titrant, with 0.5 % hydroalcoholic phenolphthalein solution and 0.1 % methyl orange as indicators). Note that, due to the very low concentration of Ca^{2+} in the bittern, it was measured by ethylenediaminetetraacetic acid (EDTA) complexometric titration, as explained in Section 2.3.

Concentration of Mg and Ca ions in the NF retentate were ~1.2 times higher than those typical of RO seawater brines. Mg^{2+} was ~16 times higher in the bittern solution than in the NF retentate, while the concentration of Ca^{2+} was ~8 times lower due to the precipitation process of Ca-compounds in the saltworks. In $Mg(OH)_2$ precipitation tests and direct carbonation tests, NaOH solutions were the alkaline reagent. NaOH solutions were prepared by dissolving analytical grade sodium hydroxide (NaOH, Honeywell Fluka > 98 %) pellets in deionized water. The concentration of hydroxyl ions (OH^-) was assessed by titration with standard hydrochloric acid (HCl) solutions (0.1 M standard HCl solutions, Sigma Aldrich). A highly pure CO_2 stream (PHARGALIS™ > 99.99 $\%_{v/v}$) was adopted in direct and indirect carbonation tests.

2.2. Experimental set-up and procedure

Indirect carbonation tests require the production of $Mg(OH)_2$ slurries as described in Section 2.2.1, while direct carbonation tests could be performed using the Mg-rich solution as it is.

2.2.1. $Mg(OH)_2$ synthesis (needed for indirect carbonation tests)

The reaction between Mg^{2+} and OH^- ions leads to the precipitation of magnesium hydroxide solids [28], according to Eq. (1):

Table 1
Concentrations of cations and bicarbonate species in the NF retentate and the bittern solution. Cations were measured by Ion chromatography (IC) and ethylenediaminetetraacetic acid (EDTA) complexometric titration techniques, while the bicarbonate content was assessed by titration following the APAT 2010 B method.

Analytical technique	Species	NF retentate Concentration (ppm)	Bittern Concentration (ppm)
IC	Na^+	18544 ± 1000	55530 ± 4335
IC	K^+	665 ± 150	12749 ± 1019
IC	Mg^{2+}	3133 ± 50	49551 ± 337
IC/EDTA	Ca^{2+}	1090 ± 30 (IC)	146 ± 3 (EDTA)
APAT 2010 B	HCO_3^-	385 ± 30	1462 ± 116

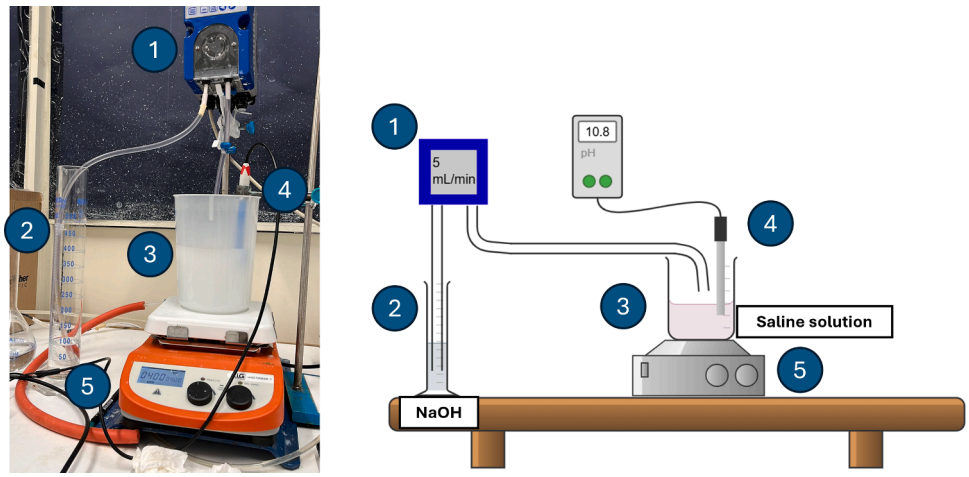

Fig. 1. A picture (a) and a scheme (b) of the single-feed semi batch system adopted for $Mg(OH)_2$ slurries production. (1) peristaltic pump; (2) graduated cylinder; (3) 1 L beaker; (4) pH-meter and (5) magnetic stirrer.

$$Mg^{2+}(aq) + 2\bullet OH^{-}(aq) \rightarrow Mg(OH)_2(s) \quad (1)$$

$Mg(OH)_2$ slurries were synthesized by adopting a single-feed semi batch system composed of (1) a peristaltic pump (Kronos 50), (2) a graduated cylinder, (3) a 1 L beaker, (4) a pHmeter (WTW™ pH/Cond 3320) and (5) a magnetic stirrer (ARGO LAB). Fig. 1.a and b show a picture and a schematic representation of the experimental set-up.

In all tests, the saline solution, either the NF retentate or the bittern, were put in the beaker, while NaOH solutions were injected into it at 5 mL/min from the graduated cylinder.

Solutions were stirred at 300 rpm. $Mg(OH)_2$ synthesis tests were conducted three times at room temperature for the sake of reproducibility. Details about the adopted operating conditions are reported in Table 2.

Cases #1-P and #2-P investigated the influence of different final pH values, namely 10.5 and 12.8, on the possible co-precipitation of calcium ions and their impact on the following carbonation step. As a matter of fact, the $Mg(OH)_2$ precipitation occurs at pH values between 9.9 and 10.8 [29]. In this pH range, calcium carbonate ($CaCO_3$) is expected to co-precipitate ($CaCO_3$(s) already precipitate at a pH value of ≥ 9 [30]), while the co-precipitation of calcium hydroxide, $Ca(OH)_2$, solids occurs at pH values higher than 12.8 [29]. Conversely, Case #3-P was conducted only at a pH value of 10.8 due to the negligible amount of Ca^{2+} in the bittern.

In Case #1-P, 2.00 M NaOH solutions were adopted. A higher volume of NaOH solution was required to reach the higher final pH value of 12.8 in Case #2-P. A volume increase, in spite of using a higher concentration NaOH solution, was selected as a preferred strategy in order to avoid safety issues and also to facilitate the possibility of using in-situ generated solutions (see Section 3.2.3). In Cases #3-P, a 1.00 M NaOH solution was adopted, as it allowed to obtain $Mg(OH)_2$ suspensions with a magma density of $\sim 22 \pm 1$ g/L. This magma density was chosen as the reference in this study since the low concentration of Mg^{2+} in the NF brine would have required too many batches to collect enough amount of $Mg(OH)_2$ suspensions with the same magma densities adopted in the literature (40 g/L, [31,32]). As a matter of fact, Cases #1-P and #2-P were repeated four times to, eventually, collect 500 mL of $Mg(OH)_2$ suspensions with a magma density of $\sim 22 \pm 1$ g/L.

In all tests, 20 mL of the slurries were taken for characterization (see section 2.4). In particular, this amount was filtered through a filtration system (NALGENE®) using glass microfiber filters with a diameter of 47 mm and a pore size of 1.6 μm (LLG LABWARE). Solids were washed using ultra-pure water to reduce the amount of entrapped mother liquor and dried for 24 h at 120 °C in an oven (ARGO LAB).

2.2.2. Carbonation tests

The indirect carbonation process involves the dissolution of available $Mg(OH)_2$ solids in a suspension, Eq. (2), due to the acidification action of the CO_2 stream in the aqueous systems. CO_2 (g) absorbs in an aqueous solution, to further react with OH^- ions forming bicarbonate species, Eq. (3). At pH higher than 8, bicarbonates lead to carbonate species Eq. (4). Finally, carbonate ions react with available Mg^{2+} ions leading to the precipitation of magnesium carbonate compounds, such as the nesquehonite, Eq. (5), [33]:

$$Mg(OH)_2(s) \rightarrow Mg^{2+}(aq) + 2\bullet OH^{-}(aq) \quad (2)$$

$$CO_2(aq) + OH^{-}(aq) \leftrightarrow HCO_3^{-}(aq) \quad (3)$$

$$HCO_3^{-}(aq) + OH^{-}(aq) \leftrightarrow CO_3^{2-}(aq) + H_2O(l) \quad (4)$$

$$Mg^{2+}(aq) + CO_3^{2-}(aq) + 3H_2O(l) \leftrightarrow MgCO_3 \bullet 3H_2O(s) \quad (5)$$

During direct carbonation processes, a CO_2 stream and a Mg^{2+}-containing solution are added, at the same time, into an alkaline solution. Mg^{2+} can react (i) with available OH^- ions, precipitating magnesium hydroxide solids, Eq. (1), that further dissociate to form magnesium carbonate, Eqs. (2–5), or (ii) with carbonate species already dissolved in the alkaline solution, Eq. (5).

Fig. 2 shows a picture and a scheme of the experimental setup adopted for direct and indirect carbonation tests.

In direct carbonation tests, 100 mL of the Margi bittern was

Table 2
Operating conditions for the synthesis of $Mg(OH)_2$ slurries. All tests were carried out at a stirring speed of 300 rpm and at room temperature. NaOH solutions were added dropwise at a flow rate of 5 mL/min. The letter P refers to $Mg(OH)_2$ precipitation tests.

Case	Saline solution	Volume of the saline solution [mL]	NaOH concentration [M]	Volume of NaOH [mL]	Final pH
#1-P	NF retentate	400 ± 5	2.00 ± 0.05	52 ± 1	10.5
#2-P	NF retentate	400 ± 5	2.00 ± 0.05	100 ± 5	12.8
#3-P	Margi bittern	100 ± 1	1.00 ± 0.05	400 ± 5	10.8

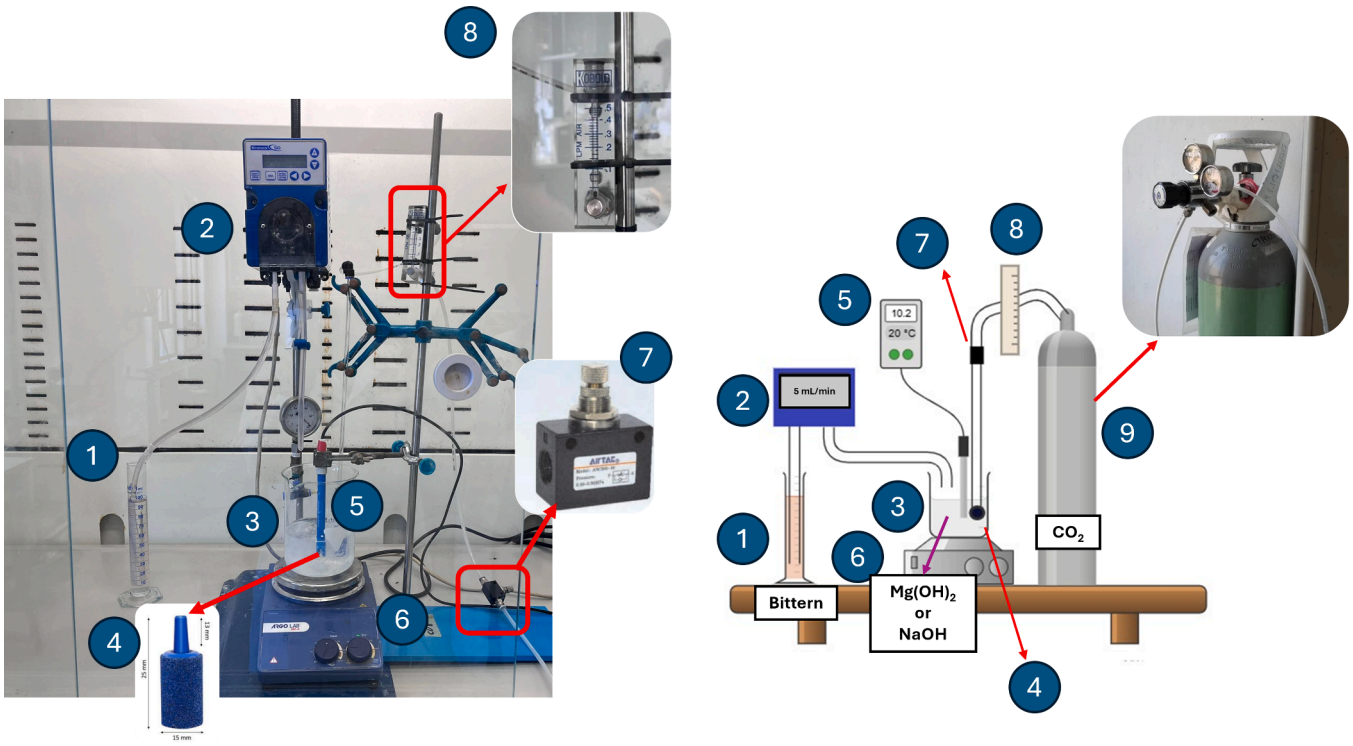

Fig. 2. A picture (a) and a scheme (b) of the experimental set-up for carbonation tests: (1) graduated 100 mL cylinder; (2) Kronos 50 peristaltic pump; (3) 1 L beaker; (4) CO_2 sparger; (5) pH meter (WTW™ pH/Cond 3320); (6) magnetic stirrer (ARGO LAB); (7) needle valve (AIRTAC) for CO_2 flow rate control; (8) rotameter; (9)CO_2 cylinder. Note that, indirect carbonation tests were conducted without the use of the peristaltic pump and the graduated cylinder, as 500 mL of $Mg(OH)_2$ slurries were loaded within the beaker.

withdrawn from a graduated cylinder at a flow rate of 5 mL/min (total pumping time of 20 minutes), by using a Kronos 50 peristaltic pump. The bittern was added into a 1 L beaker already containing 400 mL of a 1.00 M NaOH solution. The suspension was stirred at 300 rpm using a magnetic stirrer (ARGO LAB). pH and temperature were recorded by a pH meter (WTW™ pH/Cond 3320). The CO_2 flow rate was 0.4 L/min (controlled by a needle valve, AIRTAC). The CO_2 stream was injected through a sparger until the pH of the suspension reached a value of ~8 in order to avoid the dissolution of carbonates species, which would occur at pH values lower than ~8 [34].

In the case of indirect carbonation tests, the peristaltic pump and the graduated cylinder were not adopted (items 1 and 2 in Fig. 2), because 500 mL of $Mg(OH)_2$ suspensions, synthesized in tests P, were added in the beaker at the beginning of the tests. Details of conducted tests are reported in Table 3. Note that, if required, to restore the pH value of the suspensions synthesized in Cases #1-P and #2-P, a volume of 2.00 M of a NaOH solution was added before CO_2 injection.

5 mL of slurry samples were withdrawn every ~7 minutes. Samples were immediately filtered through a filtration system (NALGENE®) using glass microfiber filters with a diameter of 47 mm and a pore size of 1.6 μm (LLG LABWARE). Filtrates were further diluted 20 times in ultra-pure water to prevent any further evolution of the carbonation process. Solids samples were washed using ultra-pure water and dried for 24 h at 40 °C in an oven (ARGO LAB).

2.3. Analytical procedure and performance parameters

Magnesium and calcium ion concentrations were assessed in filtered solutions after $Mg(OH)_2$ slurry production and during carbonation tests. Mg^{2+} and Ca^{2+} concentrations were measured by ethylenediaminetetraacetic acid (EDTA) complexometric titration. The procedure was divided into two steps: (1) the total hardness (the sum of the Mg^{2+} and Ca^{2+} content) of the solution was measured using an ammonia buffer of pH 10.5, the eriochrome black T (EBT) as pH indicator, and a 0.01 M EDTA solution; (2) magnesium ions were precipitated through the addition of a 2.0 M KOH solution and the Ca^{2+} concentration was measured by using the 0.01 M EDTA solution and the Patton-Reeder indicator. The magnesium content was determined as the difference between the total hardness and the calcium content.

In $Mg(OH)_2$ synthesis tests (Cases P), Mg^{2+} and Ca^{2+} recoveries, Rec_i, were calculated as follows:

$$Rec_i = \frac{c_i^{in} - \left(c_i^{fin} \bullet \left(V_{brine} + V_{NaOH}\right) \Big/ V_{brine}\right)}{c_i^{in}} \quad (6)$$

Table 3
Volume of $Mg(OH)_2$ slurries, bittern and NaOH solutions adopted in the indirect and direct carbonation processes. Tests were carried out at room temperature. Suspensions were stirred at 300 rpm. A CO_2 flow rate of 0.4 L/min was adopted. Letters iC and dC indicate indirect and direct carbonation tests, respectively.

Case	Mg^{2+}- source solution	Volume of Mg^{2+}-source [mL]	NaOH concentration [M]	Volume of NaOH [mL]
#1-iC	$Mg(OH)_2$ from Case #1-P	500 ± 5	-	-
#2- iC	$Mg(OH)_2$ from Case #2-P	500 ± 5	-	-
#3-iC	$Mg(OH)_2$ from Case #3-P	500 ± 5	-	-
#4-dC	Margi bittern	100 ± 1	1.00 ± 0.05	400 ± 5

where c_i^{in} and c_i^{fin} are the initial and final concentrations of the *i-th* species, either Mg^{2+} or Ca^{2+}, while V_{brine} and V_{NaOH} are the volume of saline (either NF retentate or bittern) and NaOH solutions.

In the case of carbonation tests (tests iC and dC), the yield in nesquehonite solids with respect to Mg^{2+} and CO_2, $Yield_{Mg2+}^{Nesquehonite}$ and $Yield_{CO2}^{Nesquehonite}$, were evaluated as follows:

$$Yield_{Mg2+}^{Nesquehonite} = \frac{\left(n_{Mg2+}^{Initial} - n_{Mg2+}^{final}\right) \bullet molar\ percentage\ of\ nesquehonite\ in\ solids}{n_{Mg2+}^{Initial}} \quad (7)$$

$$Yield_{CO2}^{Nesquehonite} = \frac{n_{Mg2+}^{Initial} \bullet Yield_{Mg2+}^{Nesquehonite}}{n_{CO_2^{tot}}} \quad (8)$$

where $n_{Mg2+}^{Initial}$ and n_{Mg2+}^{final} are the initial and final moles of Mg ions (measured at the beginning and at the end of carbonation tests), while $n_{CO_2^{tot}}$ is the total moles of CO_2 introduced into the system during the carbonation test. The molar percentage of nesquehonite in synthesized solids was obtained by thermogravimetric analysis (TGA). Note that Eqs. (7–8) consider that one mole of Mg^{2+} reacts with one mole of CO_2(aq), as indicated in Eq. (5).

Several analytical techniques were adopted to characterize the synthesized solids. Particle purity was investigated by thermogravimetric analysis (TGA). TGA analyses were carried out at a heating rate of 10 °C/min from 30 °C to 1000 °C with a constant nitrogen flow of 20 mL/min (STA 449 F1 Jupiter analyzer, NETZSCH).

The purity of nesquehonite solids (the target compound of the present work) was calculated as the ratio between the sum of the mass losses occurring in the temperature range 25°C - 300 °C and 300°C - 600 °C (associated to the nesquehonite decomposition) and the theoretical value of 70.8 % [32]:

$$Purity_{Nesquehonite} = \frac{\Delta m_{25°C-300\ °C} + \Delta m_{300°C-600\ °C}}{70.8} \quad (9)$$

Note that, care must be placed when analysing TG plots that may present different decomposition phenomena in the same temperature intervals.

Solids were also characterized by fourier-transform infrared spectroscopy (FT-IR, Shimadzu IRTracer-100). FT-IR analysis was conducted in the range of 4000–400 cm^{-1}. Equipment setting was: a resolution of 4 cm^{-1}, 45 no. of scans and the Happ-Genzel apodization function. Particle morphology was examined by scanning electron microscopy via Scanning Electron Microscope FEI Quanta 200 FEG. A thin and uniform coating of gold was applied to make samples conductive. Elemental analysis was performed through Energy Dispersive X-ray technique (EDS). Moreover, the crystalline structure and impurities present in the powders were analysed by X-ray diffraction, XRD, technique using CuKa radiation (1.542° A, 40 KV, 100 mA) in the 2θ range of 10–70° at a step size of 1°/min by using the RIGAKU model D.MAX 2500 HK.

Table 4
Magnesium and calcium recoveries, Eq. (6), in $Mg(OH)_2$ precipitation tests (tests P).

Case	Saline solution	$Rec_{Mg^{2+}}$ [%]	$Rec_{Ca^{2+}}$ [%]
#1-P	NF retentate	96 ± 2	20 ± 4
#2-P	NF retentate	> 99	80 ± 5
#3-P	Margi bittern	97 ± 2	16 ± 4

3. Results and discussion

3.1. $Mg(OH)_2$ synthesis

Table 4 lists Mg^{2+} and Ca^{2+} recoveries, i.e. $Rec_{Mg^{2+}}$ and $Rec_{Ca^{2+}}$, Eq. (6), calculated after the synthesis of magnesium hydroxide slurries in tests P from NF retentates and Margi bitterns, respectively.

Magnesium recovery was ~96 %, > 99 % and ~97 % in Cases #1-P, #2-P and #3-P, respectively. Ca^{2+} recovery increased from ~20 % to ~80 % in Cases #1-P and #2-P when varying the final pH value of $Mg(OH)_2$ suspensions from 10.5 to 12.8 (see Table 4). Results are in accordance with data reported by Bang et al. [34]. Specifically, Bang et al. [34] obtained Mg^{2+} and Ca^{2+} recoveries of 90 % and 23 % at pH 10.5, while recoveries were 99 % and 29 % at pH 11, respectively, treating RO desalination brines with NaOH solutions. The higher Ca^{2+} recovery in Case #2-P obtained here, with respect to Bang et al. [34], can be attributed to the higher concentration of Ca^{2+} in the retentate and the possible precipitation of solids species, probably $CaCO_3$(s), that were observed floating on the liquid surface. This can be related to the interaction of the suspension at high pH with the CO_2 in the air, thus increasing the Ca^{2+} recovery. Calcium recovery was ~16 % in Case #3-P.

The FT-IR spectra of synthesized $Mg(OH)_2$ powders are reported in Fig. 3.

In all solids, the presence of $Mg(OH)_2$ compound was marked by the vibration band at 3690 cm^{-1} [36]. In Cases #1-P and #2-P, vibration peaks at 867 cm^{-1} and 1415 cm^{-1} were also observed. These peaks are related to the presence of $CaCO_3$ and $Ca(OH)_2$ species [37]. Higher peaks were noticed in samples precipitated in Case #2-P with respect to those of Case #1-P, indicating a higher amount of $CaCO_3$ and $Ca(OH)_2$ species in the solids due to the higher final pH value of the slurry. Solids of Case #3-P revealed only the peak associated to the presence of the $Mg(OH)_2$ compound. To confirm FT-IR analysis, TG plots of $Mg(OH)_2$ solids

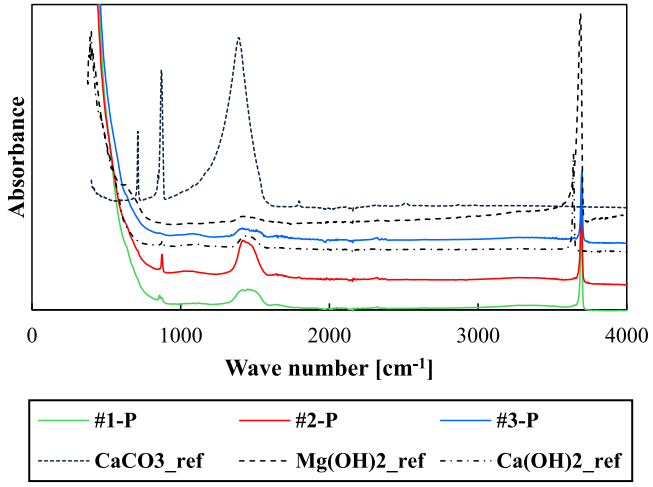

Fig. 3. FT-IR spectra of $Mg(OH)_2$ solids synthesized in Cases #1-P, #2-P and #3-P. Reference spectra for $Mg(OH)_2$, $CaCO_3$ and $Ca(OH)_2$ compounds were taken from RRUFF™ database [35].

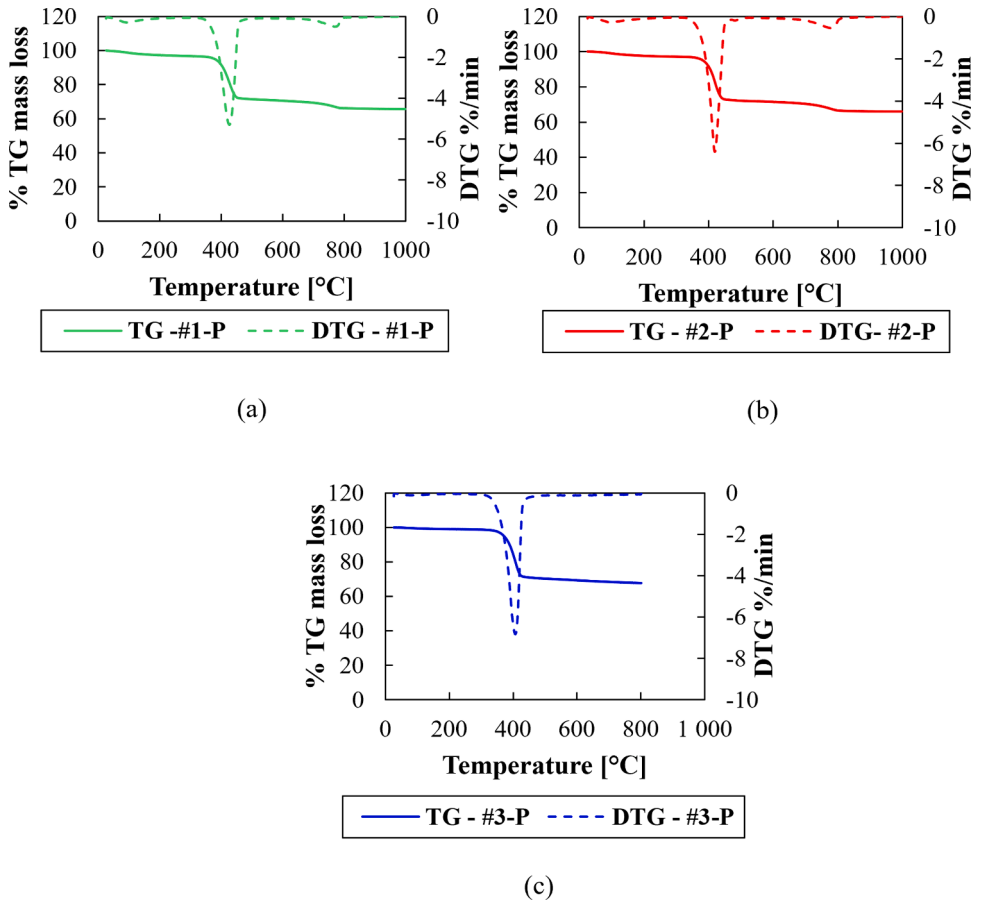

Fig. 4. TG and DTG plots of $Mg(OH)_2$ solids synthesized in Cases #1-P (a), #2-P (b) and #3-P (c).

Table 5
$Mg(OH)_2$, $CaCO_3$ and $Ca(OH)_2$ species content in solids synthesized during indirect carbonation tests.

Case	$Mg(OH)_2$ content [%]	$CaCO_3$ content [%]	$Ca(OH)_2$ content [%]
#1-P	87	13	-
#2-P	82	16	2
#3-P	> 98	-	-

are shown in Fig. 4.

Two main mass losses can be identified in TG plots of solids produced in Cases #1-P and #2-P. The first occurred in the temperature range between 300°C and 500°C, while the second between 650°C and 850°C. These two temperature mass losses are related to the $Mg(OH)_2$ and $CaCO_3$ compounds decomposition in oxide species [37,38], respectively. In Case #2-P, a very small mass loss was also detected in the temperature range between 400°C and 550°C due to the decomposition of $Ca(OH)_2$ compounds [39]. Solids precipitated in Case #3-P exhibited only the mass loss attributed to the decomposition of $Mg(OH)_2$ compounds, thus indicating the absence of $CaCO_3$ or $Ca(OH)_2$ species. The quantitative content of $Mg(OH)_2$, $CaCO_3$ and $Ca(OH)_2$ compounds in the synthesized solids determined from TG curves is reported in Table 5.

FT-IR and TG data were also confirmed by XRD spectra of solids, see Appendix A.1. Specifically, $Mg(OH)_2$ species was the dominant compound in all solids. Traces of aragonite (calcium carbonate) were detected in Case #1-P. Aragonite and calcite species were identified in samples of Case #2-P. The presence of the two calcium carbonate species can be related to the high pH environment in which the reaction occurred [40]. Traces of $Ca(OH)_2$ were also detected in solids of Case #2-P.

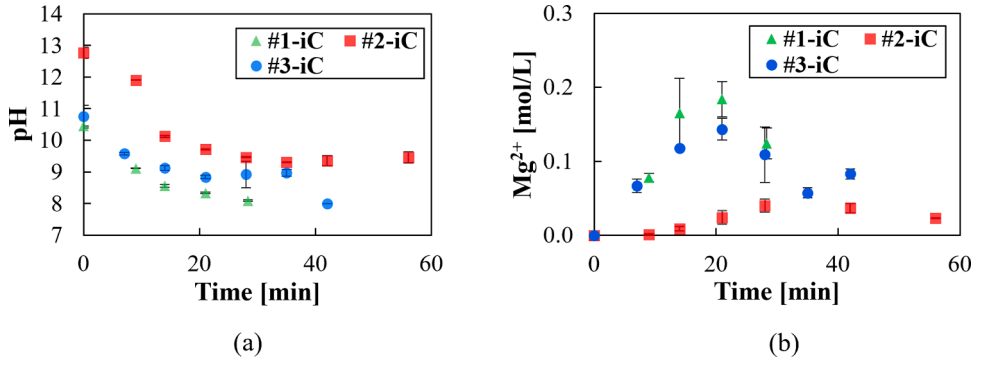

Fig. 5. pH trends and Mg^{2+} concentration trends over time for Cases #1-iC, #2-iC and #3-iC.

3.2. Direct and indirect carbonation tests

3.2.1. Indirect carbonation tests

Fig. 5.a and. b show pH trends and Mg^{2+} concentrations measured during indirect carbonation tests, namely Cases #1-iC, #2-iC and #3-iC.

Initial pH values were ~10.5, ~10.8 and ~12.8 according to the final pH value of $Mg(OH)_2$ slurries produced in Cases #1-P, #2-P and #3-P, respectively. In Case #1-iC, pH values sharply decreased to a value of ~8 within ~28 minutes. pH values fluctuated around a value of 9.35 in Case #2-iC, while pH was ~8 after 42 minutes in Case #3-iC. The pH decrease indicated the evolution of the conversion process of $Mg(OH)_2$ solids into nesquehonite ones that occurs until pH values ranges 7.8–8.2 [32,41]. Note that, at pH values lower than ~8, the dissolution of carbonates species would occur [34]. The higher pH value attained in Case #2-iC can be attributed to the presence of a high amount of calcium ions in the slurry that could cause a buffer action on the reaction system [42,43].

The Mg^{2+} concentration exhibited a non-monotonic increasing/decreasing trend with a maximum. This is due to the initial dissolution process of $Mg(OH)_2$ solids, Eq. (2), that led to an increase of the concentration of Mg^{2+} in the system until the crystallization process of nesquehonite crystals became the dominant phenomenon, consuming Mg ions. The maximum Mg^{2+} concentration values recorded at 20 mins in Cases #1-iC and #3-iC were 0.18 ± 0.02, 0.14 ± 0.01 mol/L, respectively, while a lower Mg^{2+} concentration of 0.05 ± 0.01 mol/L was attained at 28 mins in Case #3-iC. The lower Mg^{2+} concentration can be attributed to the higher pH of the solution that limits and slows the dissolution of $Mg(OH)_2$ solids, thus hindering the carbonation process. Fig. 6.a shows the FT-IR spectra of synthesized nesquehonite solids. In addition, the dynamics of the formation of nesquehonite crystals from $Mg(OH)_2$ ones observed for the Case #3-iC as a function of the reaction time is reported in Fig. 6.b.

FT-IR spectra clearly exhibited the presence of magnesium carbonate in the form of nesquehonite. The peak at 3690 cm^{-1} (presence of $Mg(OH)_2$ compounds) was almost absent for Cases #1-iC and #3-iC, while it was still present in Case #2-iC. This is in accordance with the low Mg^{2+} concentration shown in Fig. 5.b caused by the higher pH of the suspension that limited the dissolution of $Mg(OH)_2$ solids and their further conversion into Nesquehonite ones.

During the indirect carbonation process, $Mg(OH)_2$ solids slowly dissolved providing Mg^{2+} for the crystallization of nesquehonite ones. This is shown by the reduction of the peak at 3690 cm^{-1} over time (see Fig. 6.b) which almost disappeared after about 21 mins, although 42 mins were required to fully vanish. Consequently, peaks of nesquehonite crystals increased over time.

TG and DTG plots of solids produced in Cases #1-iC, #2-iC and #3-iC are shown in Fig. 7.

Different mass losses were identified in TG plots. In Case #1-iC, an initial mass loss of ~34.5 % occurred in the temperature range between 25°C to 300°C. A second mass loss equal to 27.9 % was observed from 300°C and 600 °C. These two mass losses are related to the release of water and CO_2 molecules from magnesium carbonate trihydrate species, namely the Nesquehonite [41]. In these temperature ranges, the calcination process of $Mg(OH)_2$ solids can also occur [44], however, it is difficult to be determined due to the overlap of the Nesquehonite calcination one. A third mass loss of 5.1 % was also noticed in the temperature interval between 600°C and 850 °C related to the calcination process of calcium carbonate, thus indicating the co-presence of Ca compounds in the powders [38]. Overall, the purity of nesquehonite solids calculated by using Eq. (9) was ~88 %.

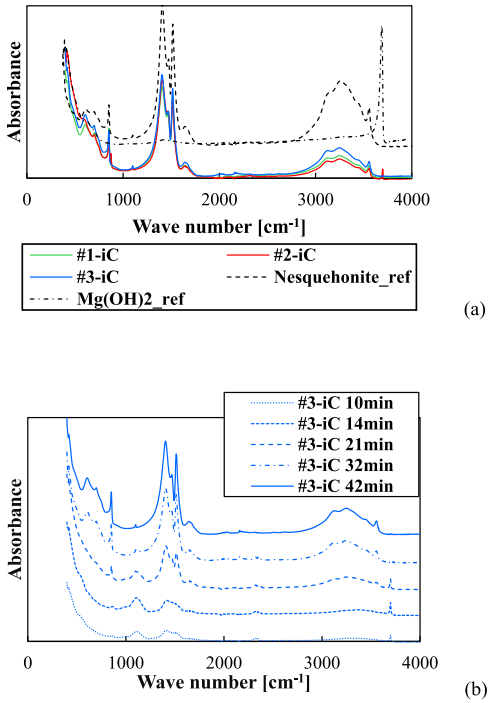

Fig. 6. – (a) FT-IR spectra of nesquehonite solids produced in Cases #1-iC, #2-iC and #3-iC. (b) FT-IR spectra of solids collected at several times during the indirect carbonation process of Case #3-IC. FT-IR spectra of $Mg(OH)_2$ and nesquehonite compounds (used as references) were taken from RRUFF™ database [35].

The TG plot of powders synthesized in the Case #2-iC showed three mass losses of ~27.9 %, ~26.3 % and ~7.3 % occurring at temperature intervals of (i) 25°C and 300°C, (ii) 300 °C and 600 °C and (iii) 600 °C and 850°C, respectively. In this case, the DTG curve showed two marked peaks at about ~400 °C and at ~530 °C, indicating the possible co-presence of $Mg(OH)_2$ (peak at ~400°C) and $Ca(OH)_2$ (peak at ~530°C) compounds [39]. The mass loss between 600°C and 850°C was again due to the presence of $CaCO_3$ compounds in the solids. In this case, it is more difficult to estimate the purity of nesquehonite solids since the mass losses due to the presence of $Mg(OH)_2$ and $Ca(OH)_2$ must be taken into account. On this bases, the purity of nesquehonite solids, Eq. (9), was estimated to be ~ 54 %.

In Case #3-iC, only the two main mass losses occurring in the temperature range of 25°C-300°C and 300–600 °C were observed, i.e. ~37.6 % and 32 %, being the purity of nesquehonite solids, Eq. (9), > 98 %.

XRD spectra, see Appendix A.2.2 confirmed the presence of nesquehonite solids. Impurities of aragonite were detected in solids of Case #1-iC, in accordance with TG data. $Mg(OH)_2$ species were identified in solids of Case #2-iC, thus confirming the influence of the high pH value in the test. No impurities were observed in XRD spectra of powders of Case #3-iC.

For all tests, the yield in nesquehonite solids with respect to Mg^{2+} and CO_2, $Yield_{Mg2+}^{Nesquehonite}$ and $Yield_{CO2}^{Nesquehonite}$, were calculated based on Eqs. (7)-(8). Specifically, $Yield_{Mg2+}^{Nesquehonite}$ was 54 %, 58 % and 78 % for

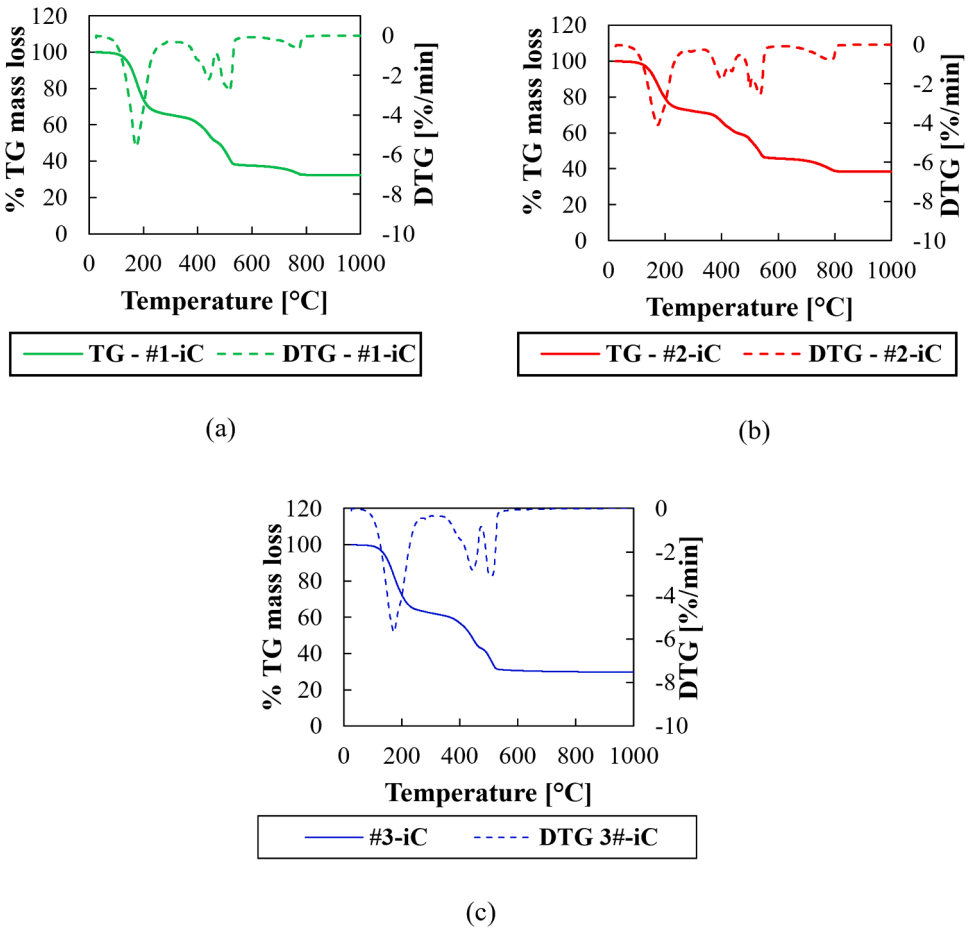

Fig. 7. TG and DTG plots of synthesized solids in Cases #1-iC (a), #2-iC (b) and #3-iC (c).

Cases #1-iC, #2-iC and #3-iC, respectively, while the $Yield_{CO2}^{Nesquehonite}$ was 22 %, 10 % and 23 %. These data agree with literature ones. Bang at al. [34] reported Mg^{2+} and CO_2 recoveries of 86 % and 12 %, respectively, treating a seawater desalination brine. The same authors improved the CO_2 yield up to 57 % by adopting sequential mineralization steps [45].

Notably, in the present work the CO_2 yield was evaluated with respect to the total CO_2 quantity insufflated in the system. Inefficiencies related to the limited CO_2 absorption, the residence time of bubbles in the system or the one-through CO_2 passage into the solution can affect the overall process. Strategies such as the use of ammine to enhance the CO_2 absorption [8] or the use of an ammonium chloride buffer [17,41] could improve the CO_2 yield in the process.

For the sake of completeness, SEM images of synthesized solids are presented in Fig. 8.

Rod or needle -like crystals of nesquehonite compounds [46] can be observed in all cases. Traces of calcium compounds were identified in solids of Cases #1-iC and #2-iC, i.e. cubic shaped crystals or ball rounded structures [47] (see Fig. 8b and e) in accordance with FT-IR, TG and XRD analysis.

The presence of Ca was also confirmed by EDS analysis, as shown in Fig. 8. c and f.

3.2.2. *Direct carbonation tests*

The pH trend and the Mg^{2+}concentration over time recorded in the Case #4-dC are shown in Fig. 9.

The pH decreased from a value of ~13 to ~8.2 at 21 mins and to ~7.8 at 23 mins. The high initial pH value was due to the presence of the NaOH solution in the beaker at the beginning of the test. Mg^{2+} concentration increased over time due to the dropwise addition of the bittern. The highest value of $\sim 0.13 \pm 0.02$ mol/L was reached at ~21 mins when also the peristaltic pump was stopped. Additional 2 minutes were necessary to decrease the pH down to the value of 7.8, indicating a total conversion of available Mg^{2+} in nesquehonite solids. Comparing Fig. 9.b and Fig. 5.b, it can be observed that the direct carbonation test was faster than the indirect ones. This can be attributed to the presence of a NaOH solution in the beaker that enhanced the absorption of CO_2 and thus the availability of carbonates ions for the nesquehonite formation. Fig. 10.a, b, c and d show the FT-IR spectrum, TG and DTG curves, and SEM images at the magnification of 4000x and 20,000 x, respectively, for the samples synthesized in Case #4-dC.

Highly pure nesquehonite crystals were synthesized. FT-IR showed the presence of only nesquehonite compounds without any peaks associated to the presence of $Mg(OH)_2$ solids. Two mass losses, one from 25 to 300 °C of ~37.7 % and a second from 300 to 600 °C of ~32.2 %, were

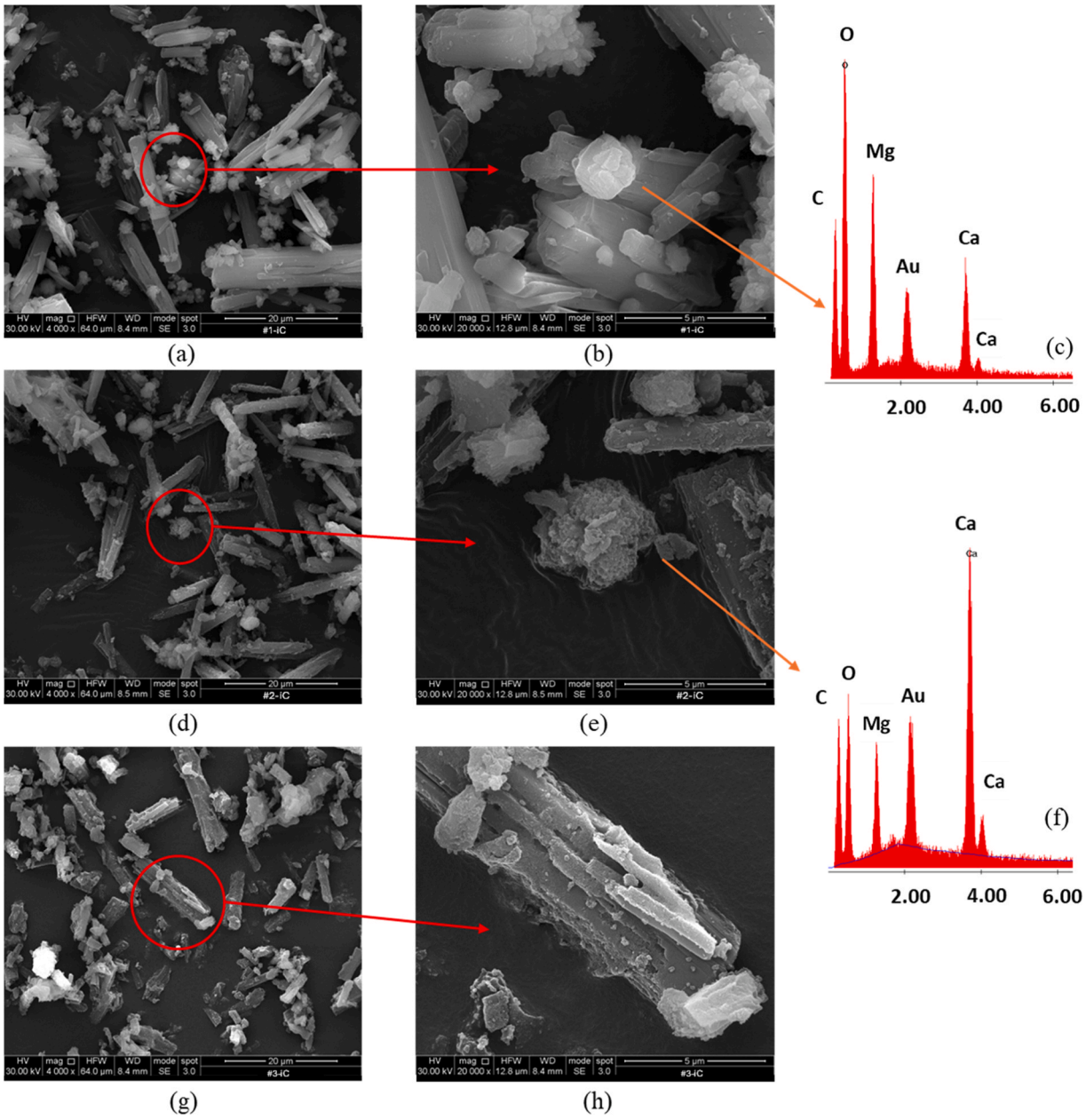

Fig. 8. SEM images of solids synthesized in Cases #1-iC (a, b), #2-iC (d, e) and #3-iC (g, h) at magnification of 4000x (a, d, g) and 20,000x (b, e, h). EDS spectra evaluated in local points of samples collected in Cases #1-iC (c) and #2-iC (f).

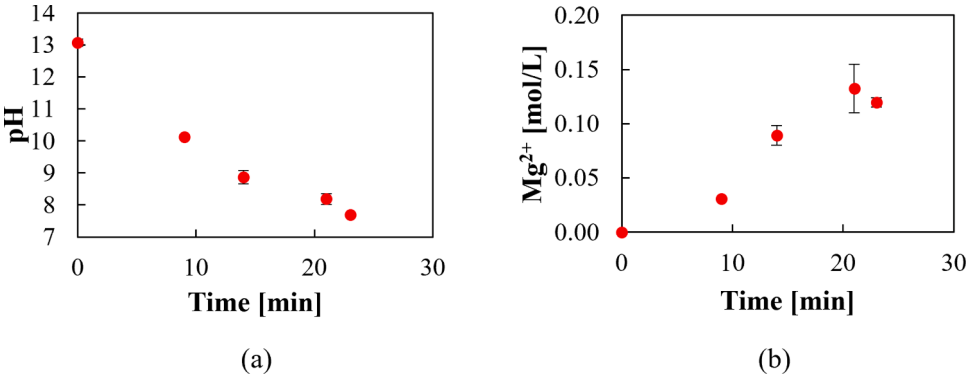

Fig. 9. (a) pH and (b) Mg^{2+} concentration trends over time for Case #4-dC.

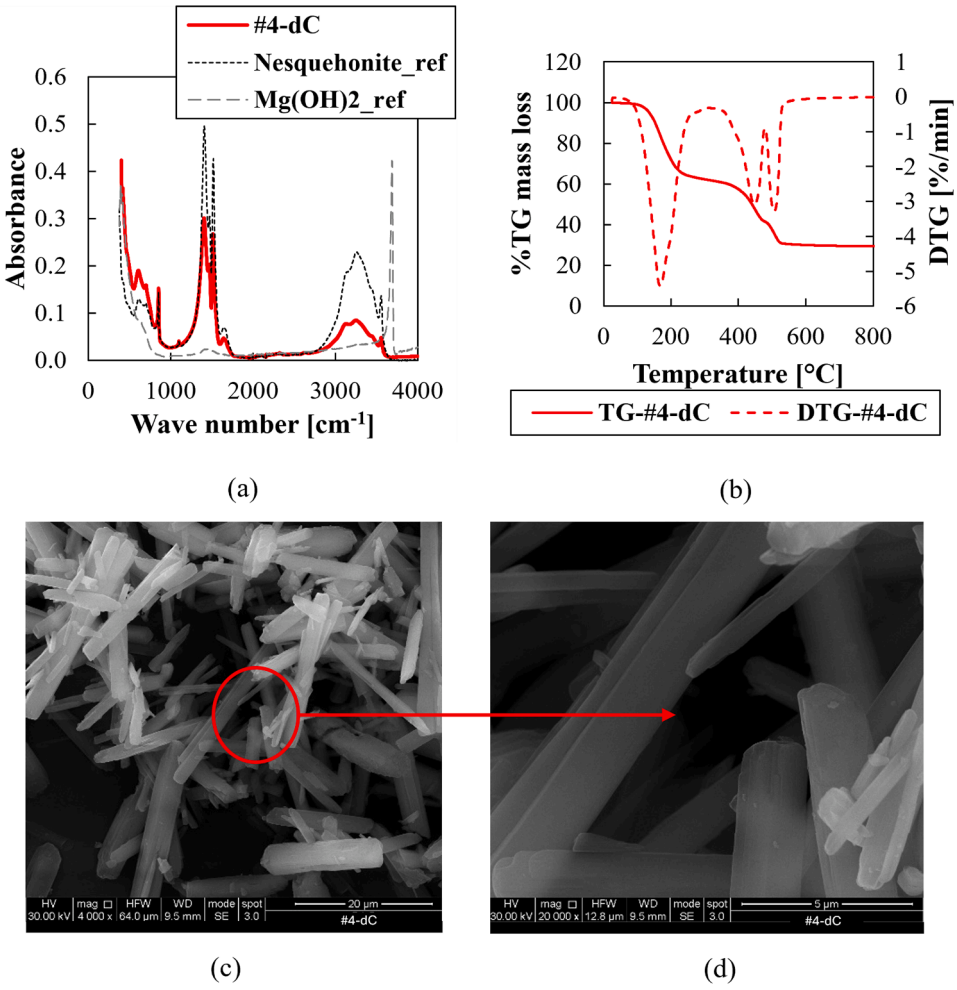

Fig. 10. (a) FT-IR spectra; (b) TG and DTG curves; SEM images at the magnification of (c) 4000x and (d) 20,000x for the solids synthesized in Case #4-dC.

Table 6
Yield in nesquehonite solids with respect to Mg^{2+} and CO_2, $Yield_{Mg2+}^{Nesquehonite}$ and $Yield_{CO2}^{Nesquehonite}$, Eqs. (7–8), and nesquehonite solids purity, $Purity_{Nesquehonite}$, Eq. (9), for all Cases here investigated. Literature data are also reported.

	Saline solution	$Yield_{Mg2+}^{Nesq.}$	$Yield_{CO2}^{Nesq.}$	$Purity_{Nesq.}$
Case #1-iC	Real seawater desalination brine	54 %	22 %	~88 %
Case #2-iC	Real seawater desalination brine	58 %	10 %	~54 %
Case #3-iC	Real bittern	78 %	23 %	> 98 %
Case #4-dC	Real bittern	69 %	37 %	~99 %
	Saline solution	**Mg^{2+} conversion ratio**	**CO_2 conversion ratio**	**Purity of hydromagnesite solids**
Bang et al. [34]	Real seawater desalination brine	86 %	12 %	< 90 % due to $CaCO_3$ traces
Bang et al. (99.9 % CO_2) [45]	Real seawater desalination brine	77 %	57 %	Not provided

observed in TG curves. The total mass loss was ~69.9 %, indicating a purity of nesquehonite powders, Eq. (9), of ~99 %. SEM images confirmed the presence of rod-like nesquehonite crystals. In this case, crystals exhibited smoother surfaces with respect to those observed in indirect carbonation tests. The presence of highly pure nesquehonite crystals was also confirmed by XRD spectroscopy, see Appendix A.2.1. Only peaks related to nesquehonite species could be detected in XRD spectra.

The yield in nesquehonite solids with respect to Mg^{2+} and CO_2, $Yield_{Mg2+}^{Nesquehonite}$ and $Yield_{CO2}^{Nesquehonite}$, Eqs. (7–8), were 69 % and 37 %, thus, marking the advantageous use of bittern solutions for the simultaneous utilization of CO_2 and the production of highly pure magnesium carbonate compounds with a better crystal morphology through the direct carbonation approach. Table 6 lists the yield in nesquehonite solids with respect to Mg^{2+} and CO_2, $Yield_{Mg2+}^{Nesquehonite}$ and $Yield_{CO2}^{Nesquehonite}$, along with

nesquehonite solids purity for all Cases #1-iC, Cases #2-iC, Cases #3-iC and Cases #4-dC. In addition, data from literature are reported for the sake of comparison.

Note that, the Mg^{2+} and CO_2 conversion adopted by Ban et al. are similar to the yields here introduced, namely Eqs. (7–8). Data in Table 6 clearly show the advantages of adopting the direct carbonation process of real bitterns for CO_2 utilization and production of highly pure compounds thanks to the higher Mg^{2+} concentration in the bittern and the lower calcium content with respect to NF retentate brines.

3.2.3. Possible applications of residual alkaline saline solution

Some considerations are required in order to fully analyse the scalability of the proposed method, looking, in particular, at the fate of the alkaline residual saline solutions, generated as a by-product of the production of nesquehonite solids from brines. Disposal or re-use of these solutions has to be considered, opening the room to several possible applications, such as:

- the alkaline solutions could be adopted for the in-situ production of required reagents, i.e. NaOH solutions, using Electrodialysis with Bipolar Membrane units. In this case, a pre-treatment of the solution would be necessary to (i) reduce their Mg^{2+} concentration, through the addition of NaOH solutions, and (ii) to extract carbonates/bicarbonates species as CO_2. The resulting $Mg(OH)_2$ solids and CO_2 could be re-used in the carbonation step. The final diluted solution, after the EDBM unit, would be rejected into the sea, without causing any environmental issues.
- If the carbonation process of saltworks bitterns is concerned, the carbonates/bicarbonates species in the alkaline solutions could be extracted via acidification and stripping processes. The recovered CO_2 could be re-used in the carbonation step, while the liquid solution could be fed back to intermediate ponds in the saltworks. This would increase the production of NaCl compounds and allow the recovery of residual Mg^{2+} through the reprocessing of the bittern.
- If a desalination industry is located near the saltworks/evaporative ponds, the alkaline solution could be used as a pre-treatment for RO/NF brines to reduce their Ca^{2+} content. $CaCO_3$ would precipitate due to the high content of bicarbonate/carbonate species in the alkaline solution. The Ca^{2+}-free solution can be employed in Zero Liquid Discharge schemes to produce highly pure-$Mg(OH)_2$ solids and enhance water recovery of desalination plants.

All these options deserve a more in-depth analysis, which will be the objective of future investigations.

4. Conclusions

In the present work, the direct and indirect carbonation processes of a real bittern collected from the Margi saltworks located in Trapani district (Sicily, Italy) were thoroughly assessed for the first time. For comparison, the indirect carbonation process of a real seawater desalination brine, outcoming the reverse osmosis desalination plant located in Tenerife island and further enriched in bivalent ions through a nanofiltration step, was studied.

First $Mg(OH)_2$ suspensions and solids were synthesized from brines at pH values of 10.5 and 12.8, and at pH of 10.8 from the bittern. Highly pure $Mg(OH)_2$ solids were produced from bitterns, while $CaCO_3$ and $Ca(OH)_2$ compounds were identified in solids synthesized from NF brines due to the co-precipitation of Ca ions. Slurries were further treated with a pure CO_2 stream (indirect carbonation process). Highly pure Nesquehonite solids were synthesized from $Mg(OH)_2$ suspensions from bitterns, while traces of $CaCO_3$ and $Ca(OH)_2$ solids were again detected among Nesquehonite crystals when using $Mg(OH)_2$ suspensions from brines. It was also observed that a higher Ca amount in $Mg(OH)_2$ slurries hindered the indirect carbonation process, probably due to the pH buffer action of Ca-compounds that slowed and limited the dissolution of $Mg(OH)_2$ solids. A maximum CO_2 yield of ~22 %, in accordance with literature data, was measured in indirect carbonation tests of $Mg(OH)_2$ suspensions synthesized from brine and bittern solutions. Conversely, CO_2 yield reached a percentage value of 37 % in direct carbonation process of the bittern solution. The direct carbonation was also the fastest approach, being at least 7 mins faster than the fastest indirect case. In addition, highly pure well-defined and surface-smooth nesquehonite crystals were synthesized.

Overall, the present study marks the advantages of adopting bittern solutions as promising sources for direct carbonation process to simultaneously utilize CO_2 streams and produce highly pure/well defined nesquehonite crystals. This is due the high Mg^{2+} content in the bittern and the pretty low Ca^{2+} content. With this respect, with the aim of reducing the environmental impact of desalination plants, the adoption of evaporation ponds to produce minerals of interest and highly concentrated Mg^{2+} rich bitterns free of Ca ions, as foreseen in the REWAISE project, is an interesting opportunity to be pursued.

CRediT authorship contribution statement

Micale Giorgio: Supervision, Resources, Project administration, Methodology, Funding acquisition, Conceptualization. **Tamburini Alessandro:** Writing – review & editing, Supervision, Resources, Project administration, Methodology, Funding acquisition, Conceptualization. **Cipollina Andrea:** Supervision, Resources, Project administration, Methodology, Funding acquisition, Conceptualization, Writing – review & editing. **Battaglia Giuseppe:** Writing – original draft, Visualization, Validation, Methodology, Investigation, Formal analysis, Data curation, Conceptualization. **Cardella Michela:** Writing – original draft, Visualization, Validation, Methodology, Investigation, Formal analysis, Data curation.

Declaration of Competing Interest

The authors declare that they have no known competing financial interests or personal relationships that could have appeared to influence the work reported in this paper.

Acknowledgements

This project has received funding from the European Union's Horizon 2020 Research and Innovation Programme under Grant Agreement No. 869467 (SEArcularMINE). This output reflects only the author's view. The European Health and Digital Executive Agency (HaDEA) and the European Commission cannot be held responsible for any use that may be made of the information contained therein. The Authors thank the European Union and the Horizon 2020 Research and Innovation Framework Programme for funding this research under the project REWAISE grant agreement No. 869496. The Authors are also thankful to Aqualia company for having provided the nanofiltration retentate.

Appendix A

A.1 XRD spectra of solids produced in $Mg(OH)_2$ synthesis tests.

The XRD spectra of solids synthesized in Cases #1-P, #2-P and #3-P are shown in Figure A. 1 a, b and c, respectively.

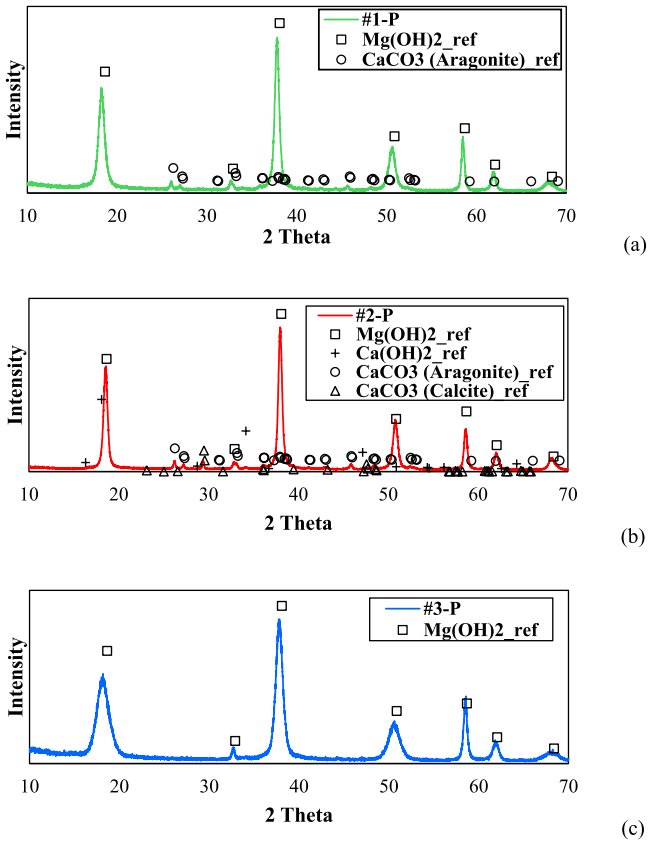

Figure A.1. XRD spectra of solids produced in Cases #1-P (a), #2-P (b) and #3-P (c). Reference spectra of $Mg(OH)_2$, $Ca(OH)_2$, $CaCO_3$ (either calcite or aragonite) species were taken from RRUFF™ database [35]

$Mg(OH)_2$, i.e. brucite, was the dominant phase in all solids. Sample #3-P exhibited only peaks attributed to $Mg(OH)_2$ solids, thus indicating a high purity of the powders. Peaks of $CaCO_3$ species, in the form of aragonite, were detected in powders produced in Case #1-P. $CaCO_3$ as aragonite and calcite species were identified in samples of Case #2-P. The presence of calcite was observed mainly due to the peak at ~29.48, among the others. The peak at ~34.15 was related to the possible presence of $Ca(OH)_2$ in the solids. XRD spectra agreed well with TG and FT-IR data discussed in Section 3.1.

A.2 XRD spectra of solids produced in carbonation tests.

A.2.1 Direct carbonation tests

Figure A. 2 shows the XRD spectrum of solids produced in Case #4-dC.

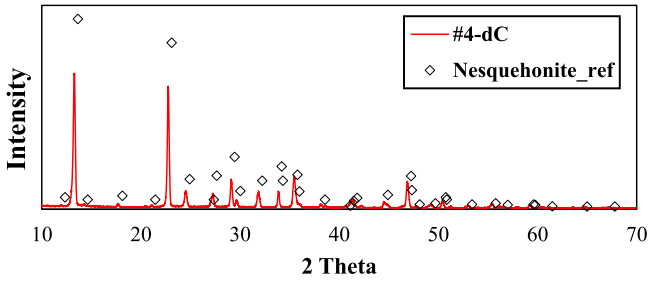

Figure A.2. XRD spectrum of powders produced in direct carbonation tests of real bittern solutions (Case #4-dC). The reference spectrum of $MgCO_3 \cdot 3\,H_2O$ (nesquehonite) species was taken from RRUFF™ database [35]

Only peaks ascribed to the presence of Nesquehonite species can be observed in Figure A. 2, indicating a high purity of the powders.

A.2.2 Indirect carbonation tests

Figure A. 3 a, b and c report XRD spectra of solids obtained in Cases #1-iC, #2-iC and #3-iC, respectively.

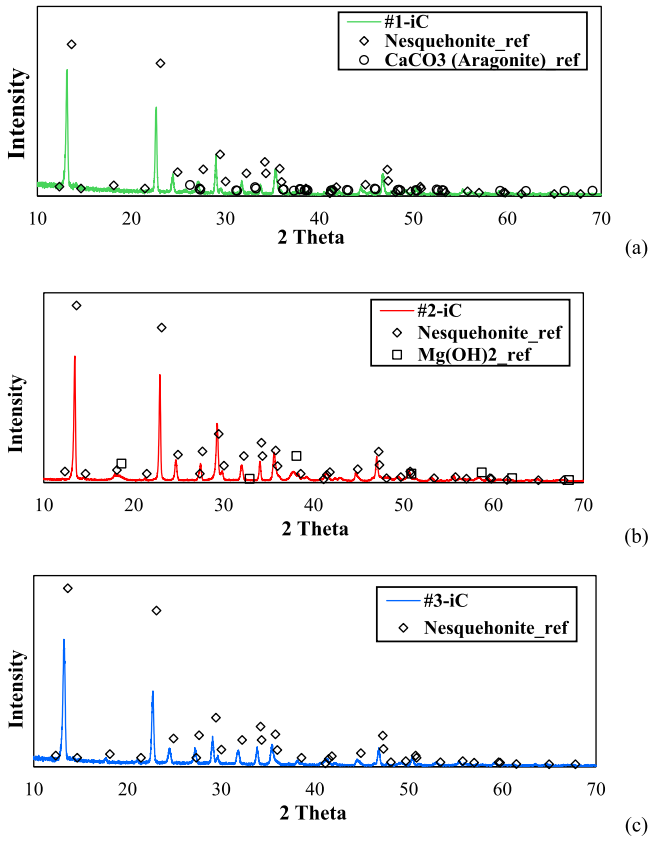

Figure A.3. XRD spectra of solids collected in Cases #1-iC (a), #2-iC (b), #3-iC (c). Reference spectra of $Mg(OH)_2$, $CaCO_3$ (aragonite), $MgCO_3 \cdot 3\ H_2O$ (nesquehonite) species were taken from RRUFF™ database [35]

Peaks related to the presence of nesquehonite species were found in all spectra of Cases #1-iC, #2-iC, #3-iC. No other peaks, thus impurities, were observed in solids of Case #3-iC. On the other hand, aragonite and $Mg(OH)_2$ traces were detected in solids of Cases #1-iC and #2-iC, respectively.

Data availability

Data will be made available on request.

References

[1] I.S. Report, Summ. Policy Intergov. Panel Clim. Change (2023), https://doi.org/10.59327/IPCC/AR6-9789291691647.001.
[2] E. Benhelal, G. Zahedi, E. Shamsaei, A. Bahadori, Global strategies and potentials to curb CO2 emissions in cement industry, J. Clean. Prod. 51 (2013) 142–161, https://doi.org/10.1016/j.jclepro.2012.10.049.
[3] E. Union, The European Green Deal, (n.d.). ⟨https://commission.europa.eu/strategy-and-policy/priorities-2019-2024/european-green-deal_en⟩ (accessed November 10, 2024).
[4] E. Jones, M. Qadir, M.T.H. van Vliet, V. Smakhtin, S. mu Kang, The state of desalination and brine production: a global outlook, Sci. Total Environ. 657 (2019) 1343–1356, https://doi.org/10.1016/j.scitotenv.2018.12.076.
[5] J.C.M. Pires, F.G. Martins, M.C.M. Alvim-Ferraz, M. Simões, Recent developments on carbon capture and storage: an overview, Chem. Eng. Res. Des. 89 (2011) 1446–1460, https://doi.org/10.1016/j.cherd.2011.01.028.
[6] M.E. Boot-Handford, J.C. Abanades, E.J. Anthony, M.J. Blunt, S. Brandani, N. Mac Dowell, J.R. Fernández, M.C. Ferrari, R. Gross, J.P. Hallett, R.S. Haszeldine, P. Heptonstall, A. Lyngfelt, Z. Makuch, E. Mangano, R.T.J. Porter, M. Pourkashanian, G.T. Rochelle, N. Shah, J.G. Yao, P.S. Fennell, Carbon capture and storage update, Energy Environ. Sci. 7 (2014) 130–189, https://doi.org/10.1039/c3ee42350f.
[7] H.J. Ho, A. Iizuka, Mineral carbonation using seawater for CO2 sequestration and utilization: a review, Sep. Purif. Technol. 307 (2023), https://doi.org/10.1016/j.seppur.2022.122855.
[8] J. Mustafa, A.A.H.I. Mourad, A.H. Al-Marzouqi, M.H. El-Naas, Simultaneous treatment of reject brine and capture of carbon dioxide: a comprehensive review, Desalination 483 (2020), https://doi.org/10.1016/j.desal.2020.114386.
[9] H.J. Ho, A. Iizuka, E. Shibata, T. Ojumu, Circular indirect carbonation of coal fly ash for carbon dioxide capture and utilization, J. Environ. Chem. Eng. 10 (2022), https://doi.org/10.1016/j.jece.2022.108269.
[10] O. Ahmed, S. Ahmad, S.K. Adekunle, Carbon dioxide sequestration in cementitious materials: a review of techniques, material performance, and environmental impact, J. CO2 Util. 83 (2024), https://doi.org/10.1016/j.jcou.2024.102812.
[11] A. Kastrinakis, V. Skliros, P. Tsakiridis, M. Perraki, CO2-Mineralised Nesquehonite: A New "Green" Building Material, in: MDPI AG, 2021: p. 60. https://doi.org/10.3390/materproc2021005060.
[12] Y. Wang, J. Liu, T. Shi, C. Li, Q. Wang, J. Zhang, Y. Zhu, X. Li, Z. Yuan, W. Yin, Synthesis and pore structure construction mechanism of porous nesquehonite, Powder Technol. 398 (2022), https://doi.org/10.1016/j.powtec.2022.117154.
[13] J.L. Gálvez-Martos, A. Elhoweris, A. Hakki, Y. Al-Horr, Techno-economic assessment of a carbon capture and utilization process for the production of plaster-like construction materials, J. CO2 Util. 38 (2020) 59–67, https://doi.org/10.1016/j.jcou.2019.12.017.
[14] L. Haurie, A.I. Fernández, J.I. Velasco, J.M. Chimenos, J.M.L. Cuesta, F. Espiell, Synthetic hydromagnesite as flame retardant. Evaluation of the flame behaviour in a polyethylene matrix, Polym. Degrad. Stab. 91 (2006) 989–994, https://doi.org/10.1016/j.polymdegradstab.2005.08.009.
[15] M. Hänchen, V. Prigiobbe, R. Baciocchi, M. Mazzotti, Precipitation in the Mg-carbonate system-effects of temperature and CO2 pressure, Chem. Eng. Sci. 63 (2008) 1012–1028, https://doi.org/10.1016/j.ces.2007.09.052.
[16] W. CHENG, Z. LI, G.P. Demopoulos, Effects of temperature on the preparation of magnesium carbonate hydrates by reaction of MgCl2 with Na2CO3, Chin. J. Chem. Eng. 17 (2009) 661–666, https://doi.org/10.1016/S1004-9541(08)60260-8.
[17] W. Wang, M. Hu, Y. Zheng, P. Wang, C. Ma, CO2 fixation in Ca2+ -/Mg2+ -rich aqueous solutions through enhanced carbonate precipitation, Ind. Eng. Chem. Res. 50 (2011) 8333–8339, https://doi.org/10.1021/ie1025419.
[18] I. Singh, R. Hay, K. Celik, Recovery and direct carbonation of brucite from desalination reject brine for use as a construction material, Cem. Concr. Res. 152 (2022), https://doi.org/10.1016/j.cemconres.2021.106673.
[19] I. Singh, K. Celik, Influence of supercritical carbon dioxide (scCO2) curing on carbonation and strength development of brucite recovered from desalination reject brine, J. CO2 Util. 79 (2024), https://doi.org/10.1016/j.jcou.2023.102657.
[20] J.H. Bang, S.C. Chae, K. Song, S.W. Lee, Optimizing experimental parameters in sequential CO2 mineralization using seawater desalination brine, Desalination 519 (2022), https://doi.org/10.1016/j.desal.2021.115309.

[21] W. Pan, Y. Yang, D. Yang, M. Arowo, S. Wu, Y. He, Q. Zeng, A novel eco-friendly circular approach to comprehensive utilizing bittern waste and oyster shell, Processes 11 (2023), https://doi.org/10.3390/pr11041209.
[22] D. Zhang, Y. Li, J. Cao, Efficient magnesium recovery from seawater desalination brine via CO2 mineralization to synthesize hydromagnesite for uranium extraction, Desalination (2023) 116629, https://doi.org/10.1016/j.desal.2023.116629.
[23] S. Lu, W. Cui, R. Wang, C. Zhang, P. Yan, Biomimetic mineralization and characterization of hierarchically structured hydrated magnesium carbonates: the effects of sodium alginate, J. CO2 Util. 56 (2022), https://doi.org/10.1016/j.jcou.2021.101848.
[24] REWAISE Project, (n.d.). ⟨https://rewaise.eu/the-project/⟩ (accessed June 4, 2024).
[25] SEArcularMINE, (n.d.). ⟨https://searcularmine.eu/⟩ (accessed September 25, 2023).
[26] A. Roa, J. López, G. Battaglia, A. Cipollina, J.L. Cortina, Integration of layer-by-layer hollow-fibre nanofiltration membranes and crystallization for water reclamation and resource recovery from acidic mine waters, Desalination 590 (2024), https://doi.org/10.1016/j.desal.2024.117960.
[27] G. Battaglia, L. Ventimiglia, F. Vicari, A. Tamburini, A. Cipollina, G. Micale, Characterization of Mg(OH)2 powders produced from real saltworks bitterns at a pilot scale, Powder Technol. 443 (2024), https://doi.org/10.1016/j.powtec.2024.119918.
[28] S. Romano, S. Trespi, R. Achermann, G. Battaglia, A. Raponi, D. Marchisio, M. Mazzotti, G. Micale, A. Cipollina, The role of operating conditions in the precipitation of magnesium hydroxide hexagonal platelets using NaOH solutions, Cryst. Growth Des. 23 (2023) 6491–6505, https://doi.org/10.1021/acs.cgd.3c00462.
[29] F. Vassallo, D. La Corte, N. Cancilla, A. Tamburini, M. Bevacqua, A. Cipollina, G. Micale, A pilot-plant for the selective recovery of magnesium and calcium from waste brines, Desalination 517 (2021) 115231, https://doi.org/10.1016/j.desal.2021.115231.
[30] S. Casas, C. Aladjem, E. Larrotcha, O. Gibert, C. Valderrama, J.L. Cortina, Valorisation of Ca and Mg by-products from mining and seawater desalination brines for water treatment applications, J. Chem. Technol. Biotechnol. 89 (2014) 872–883, https://doi.org/10.1002/jctb.4326.
[31] A. Botha, C.A. Strydom, Preparation of a magnesium hydroxy carbonate from magnesium hydroxide, Hydrometallurgy 62 (2001) 175–183, https://doi.org/10.1016/S0304-386X(01)00197-9.
[32] B. Han, H. Qu, H. Niemi, Z. Sha, M. Louhi-Kultanen, Mechanistic study of magnesium carbonate semibatch reactive crystallization with magnesium hydroxide and CO2, Ind. Eng. Chem. Res. 53 (2014) 12077–12082, https://doi.org/10.1021/ie501706j.
[33] J.L. Galvez-Martos, A. Elhoweris, J. Morrison, Y. Al-Horr, Conceptual design of a CO2 capture and utilisation process based on calcium and magnesium rich brines, J. CO2 Util. 27 (2018) 161–169, https://doi.org/10.1016/j.jcou.2018.07.011.
[34] J.H. Bang, Y. Yoo, S.W. Lee, K. Song, S. Chae, Co2 mineralization using brine discharged from a seawater desalination plant, Minerals 7 (2017), https://doi.org/10.3390/min7110207.
[35] B. Lafuente, R.T. Downs, H. Yang, N. Stone, The power of databases: The RRUFF project, n.d.
[36] M. Sichov, K. Boriak, L. Kolomiets, Technology for obtaining highpure magnesium compounds using the hydrolytic processes of sedimentation, East. -Eur. J. Enterp. Technol. 1 (2022) 43–52, https://doi.org/10.15587/1729-4061.2022.253544.
[37] Z. Du, E.H. Yang, C. Unluer, Investigation of the properties of Mg(OH)2 extracted from magnesium-rich brine via the use of an industrial by-product, Cem. Concr. Compos 152 (2024), https://doi.org/10.1016/j.cemconcomp.2024.105658.
[38] H. Dong, C. Unluer, E.H. Yang, A. Al-Tabbaa, Recovery of reactive MgO from reject brine via the addition of NaOH, Desalination 429 (2018) 88–95, https://doi.org/10.1016/j.desal.2017.12.021.
[39] J. Chang, Y. Li, M. Cao, Y. Fang, Influence of magnesium hydroxide content and fineness on the carbonation of calcium hydroxide, Constr. Build. Mater. 55 (2014) 82–88, https://doi.org/10.1016/j.conbuildmat.2013.12.099.
[40] F. Liendo, M. Arduino, F.A. Deorsola, S. Bensaid, Factors controlling and influencing polymorphism, morphology and size of calcium carbonate synthesized through the carbonation route: a review, Powder Technol. 398 (2022), https://doi.org/10.1016/j.powtec.2021.117050.
[41] V. Ferrini, C. De Vito, S. Mignardi, Synthesis of nesquehonite by reaction of gaseous CO2 with Mg chloride solution: its potential role in the sequestration of carbon dioxide, J. Hazard. Mater. 168 (2009) 832–837, https://doi.org/10.1016/j.jhazmat.2009.02.103.
[42] B. Coto, C. Martos, J.L. Peña, R. Rodríguez, G. Pastor, Effects in the solubility of CaCO 3: experimental study and model description, Fluid Phase Equilib. 324 (2012) 1–7, https://doi.org/10.1016/j.fluid.2012.03.020.
[43] S. Oxana, P. Igor, BUFFER PROPERTIES OF THE SYSTEM "CALCIUM CARBONATE-SOIL SOLUTION," (n.d.). chrome-extension://efaidnbmnnnibpcajpcglclefindmkaj/https://ibn.idsi.md/sites/default/files/imag_file/318-322_7.pdf.
[44] X.F. Wu, G.S. Hu, B.B. Wang, Y.F. Yang, Synthesis and characterization of superfine magnesium hydroxide with monodispersity, J. Cryst. Growth 310 (2008) 457–461, https://doi.org/10.1016/j.jcrysgro.2007.10.025.
[45] J.H. Bang, S.C. Chae, S.W. Lee, J.W. Kim, K. Song, J. Kim, W. Kim, Sequential carbonate mineralization of desalination brine for CO2 emission reduction, J. CO2 Util. 33 (2019) 427–433, https://doi.org/10.1016/j.jcou.2019.07.020.
[46] C. Wenting, Z. Li, Precipitation of nesquehonite from homogeneous supersaturated solutions, Cryst. Res. Technol. 44 (2009) 937–947, https://doi.org/10.1002/crat.200900286.
[47] M.C. Reis, M.F.B. Sousa, F. Alobaid, C.A. Bertran, Y. Wang, A two-fluid model for calcium carbonate precipitation in highly supersaturated solutions, Adv. Powder Technol. 29 (2018) 1571–1581, https://doi.org/10.1016/j.apt.2018.03.022.